Available online at www.sciencedirect.com
SCIENCE DIRECT®
ELSEVIER
International Journal of Solids and Structures 43 (2006) 5736–5749
INTERNATIONAL JOURNAL OF SOLIDS and STRUCTURES
www.elsevier.com/locate/ijsolstr

The effect of contact conditions and material properties on the elasticity terminus of a spherical contact

V. Brizmer, Y. Kligerman, I. Etsion *

Department of Mechanical Engineering, Technion, Israel Institute of Technology, Haifa 32000, Israel

Received 9 May 2005; received in revised form 5 July 2005
Available online 12 September 2005

Abstract

The fundamental problem of elastic–plastic normally loaded contact between a deformable sphere and a rigid flat is analyzed under perfect slip and full stick conditions for a wide range of the sphere mechanical properties. The effect of these properties on failure inception is investigated by finding the critical interference and normal loading as well as the location of the first plastic yield or brittle failure. The analysis is based on the analytical Hertz solution under frictionless slip condition and on a numerical solution under stick condition. The failure inception is determined by using either the von Mises criterion of plastic yield or the maximum tensile stress criterion of brittle failure. For small values of the Poisson's ratio the behavior in stick, when high tangential stresses prevail in the contact interface, is much different than in slip. For high values of the Poisson's ratio the tangential stresses under stick condition are low and the behavior of the failure inception in stick and slip is similar.

Keywords: Spherical contact; Plastic yield; Brittle failure; Contact conditions

1. Introduction

The contact of a sphere and a flat is a fundamental problem in contact mechanics with important scientific and technological aspects. The subject of normally loaded spherical contact stems from the classical work of Hertz in 1881 who derived an analytical solution for the frictionless (i.e., perfect slip) contact of two elastic spheres, (see Johnson, 1985). The stress field associated with elastic spherical contact was calculated in detail by Huber in 1904 (see Fischer-Cripps, 2000). The Hertz model of a perfect slip contact may

* Corresponding author. Tel.: +972 4 829 2096; fax: +972 44 832 4533.
E-mail address: etsion@tx.technion.ac.il (I. Etsion).

0020-7683/$ - see front matter © 2005 Elsevier Ltd. All rights reserved.
doi:10.1016/j.ijsolstr.2005.07.034

Nomenclature

a	contact area radius
C_v	p_{mc}/Y
E	Young's modulus of the sphere
F	failure tensile strength of the sphere material
L	load in stick
p	contact pressure
p_m	maximum contact pressure
P	load in slip
R	radius of the sphere
r,θ,z	cylindrical coordinates
Y	yield strength of the sphere material
z_0	location of yielding inception
δ	interference in stick
v	Poisson's ratio of the sphere
σ_r	radial stress
σ_1, σ_2, σ_3	principal stresses
σ_θ	circumferential stress
σ_z	normal stress in the load direction
σ_{eq}	von Mises equivalent stress
σ^+_{max}	maximum tensile stress
τ_{rz}	tangential stress
ω	interference in slip
ζ_0	dimensionless yielding inception depth, z_0/a
ζ^*_0	yielding inception depth ratio

Subscripts

c	critical value at yield inception
cf	critical value at brittle failure inception

also be valid in certain cases of frictional contact. If, for instance, two identical spheres come to a normal contact, their corresponding radial displacements at the interface are identical thus, preventing any tangential stresses there (see Johnson, 1985). Therefore, a normal contact of two identical spheres in stick can be modeled by a perfect slip (frictionless) contact between them or between a deformable sphere and a rigid flat. This idea was used extensively in modeling spherical contact under combined normal and tangential loading (for example, Mindlin, 1949; Bryant and Keer, 1982; Hamilton, 1983; Chang et al., 1988; Kogut and Etsion, 2003). In all of these works the contact is assumed in perfect slip during the normal loading but since the tangential loading can not be supported by such perfect slip the contact condition must change prior to applying the tangential load. This is done either by assuming a certain friction coefficient and a local Coulomb friction law (Mindlin, 1949; Bryant and Keer, 1982; Hamilton, 1983; Zhang et al., 2003) or by some mixed slip/stick conditions (Chang et al., 1988; Kogut and Etsion, 2003) for analyzing sliding inception based on the von Mises criterion of plastic yield.

Since a realistic contact of a sphere and flat may be far from the ideal assumption of perfect slip, and since the end of elasticity of brittle materials is different from that of ductile ones it seems appropriate to analyze this contact problem under stick condition for different material properties, and to compare

the results with the idealized solutions of perfect slip. We shall begin by reviewing the existing literature for both slip and stick contact conditions of the relevant contact problem.

Chang (1986) (see also Chang et al., 1988) solved the problem of yield inception of a spherical contact in the case of perfect slip using the stress field of Huber and the von Mises yield criterion. He calculated the critical interference at the inception of plastic deformation as a function of the mechanical properties and the radius of the sphere. Chang also presented the location of the first yield inside the sphere as a function of the Poisson's ratio. The evolution of an elastic–plastic contact between a sphere and a rigid flat with increasing interference under perfect slip condition was studied numerically by Kogut and Etsion (2002) and then by Jackson and Green (2005), who introduced an empirical equation for the critical interference at the inception of yield, somewhat different than this given by Chang (1986) and Chang et al. (1988). Etsion et al. (2005) studied the process of loading–unloading of an elastic–plastic loaded sphere in contact with a rigid flat under perfect slip condition. They calculated the contact load, stresses and deformations in the sphere during both loading and unloading, for a wide range of interferences and a variety of ductile material properties. The conditions required to initiate a brittle material failure of a spherical contact under perfect slip were studied by Fischer-Cripps (1997) and this subject is well described in Fischer-Cripps (2000).

The first analytical solution of the spherical contact problem under full stick condition is by Goodman (1962). Goodman found a simplified solution for the tangential stress distribution over the contact area of two dissimilar elastic spheres in normal contact in stick. The effect of these tangential stresses on the normal displacements was neglected, so that the pressure distribution over the contact area was assumed to be Hertzian. A more exact analysis under full stick contact condition was made by Spence (1968) who solved simultaneously the dual integral equations for shear stresses and pressure distribution over the contact area and calculated the total compressive load. It follows from Spence results that for small values of the Poisson's ratio the influence of shear stresses on the contact load is appreciable. Spence (1975) extended his previous analysis to the case of partial stick using a certain value of friction coefficient. More recently Zhupanska and Ulitko (2005) used a similar approach to solve the contact problem of a rigid cylinder indenting an elastic half-space. The cases of contact with a finite friction, and more specifically with full stick condition were considered. Johnson et al. (1973) extended the solution by Goodman (1962), and found the radial stress distribution on the surface of the sphere both inside and outside the contact interface. They solved the problem for the maximum tensile stress which causes fracture of brittle materials. Another extension of the Goodman's solution is by Hills and Sackfield (1987) that gave a complete picture of the stress distribution assuming full and partial stick contact conditions. Kosior et al. (1999) analyzed an elastic spherical contact under partial slip condition (with a finite Coulomb friction) using a domain decomposition method coupled with boundary element method. They calculated the stress distribution, the contact radius and the displacement as functions of the sphere's mechanical properties. Their results were in good agreement with the analytical solution of Spence (1975).

An extensive review of the literature on spherical and cylindrical contacts under normal load with and without friction was made by Adams and Nosonovsky (2000) including the subject of yielding inception of normally loaded spherical contact. It can be seen from this review, as well as from the above introduction, that most of the existing literature on elasticity terminus of spherical contact concern ductile materials and perfect slip contact condition. Very little work was done so far on the more realistic case of spherical contact under stick condition, and the few published solutions are either approximate or very complicated. An accurate analysis that predicts failure inception under full stick condition is still missing.

The main goal of this paper is to fill this knowledge gap and analyze and compare the ductile material yielding inception and the brittle material failure inception for the two different contact conditions (full stick or perfect slip) between a smooth elastic sphere and rigid flat.

2. The spherical contact model

Fig. 1 presents a deformable sphere in contact with a rigid flat. The solid and dashed lines show the contours of the contacting bodies after and before the loading, respectively. The interference, ω and contact area with a radius a (see Fig. 1), correspond to a contact load P. Both ω and a are assumed to be much smaller than the sphere radius R.

The material of the sphere is assumed to be isotropic and elastic until the first yield or failure is reached. Ductile and brittle models of behavior are considered separately.

Since the problem is axisymmetric, it is sufficient to consider only half of the axisymmetric hemisphere section, as shown in Fig. 1. The boundary conditions consist of constrain in the vertical and radial directions at the bottom of the hemisphere and in the radial direction at the axis of symmetry (see Fig. 1). The surface of the sphere is free elsewhere except for tractions imposed by the contacting rigid flat.

Two different types of the contact conditions are considered: perfect slip and full stick. The former case assumes no tangential stresses in the contact area. The condition of full stick implies that contacting points of the sphere and the flat (which initially lied outside the contact area and were free to acquire a relative displacement) that are overtaken by the expanding contact zone, are prevented from further relative displacement (see Johnson et al., 1973).

3. Analytical solution for perfect slip condition

The Hertz solution (see Johnson, 1985) provides the following expressions for the contact load, P, and the contact radius, a:

$$P = \frac{4}{3}\frac{ER^{1/2}\omega^{3/2}}{(1-\nu^2)} \tag{1}$$

$$a = \sqrt{\omega R} \tag{2}$$

where E and ν are the Young modulus and the Poisson's ratio of the sphere material, respectively.

The assumed parabolic distribution of the contact pressure according to Hertz is

$$p(r) = \frac{p_m}{a}(a^2 - r^2)^{1/2} \tag{3}$$

where r is a radial distance measured from the center of the contact area, and p_m, the maximum contact pressure at the center of the contact, which is given by

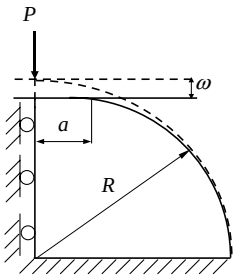

Fig. 1. A deformable sphere in contact with a rigid flat before and after loading.

$$p_{\mathrm{m}} = \frac{3P}{2\pi a^2} \tag{4}$$

The stress field along the z-axis (normal to the contact area at its center) may be written in the form (see Johnson, 1985)

$$\begin{aligned}
&\frac{\sigma_{\mathrm{r}}}{p_{\mathrm{m}}} = -(1+v)\left[\left(1-\frac{z}{a}\tan^{-1}(a/z)\right)\right] + \frac{1}{2}\left(1+\frac{z^2}{a^2}\right)^{-1} \\
&\sigma_\theta = \sigma_r \\
&\frac{\sigma_z}{p_{\mathrm{m}}} = -\left(1+\frac{z^2}{a^2}\right)^{-1} \\
&\tau_{rz} = \tau_{r\theta} = \tau_{z\theta} = 0
\end{aligned} \tag{5}$$

where σ_{r}, σ_θ and σ_z are the normal stresses in radial, circumferential and vertical directions, respectively. τ_{rz}, $\tau_{r\theta}$ and $\tau_{z\theta}$ are the corresponding shear stresses that vanish along the z-axis.

3.1. Yielding inception of ductile materials ($0.2 \leqslant v \leqslant 0.5$)

The von Mises yield criterion is used to study the inception of plastic deformation for the case of ductile materials where the Poisson's ratio varies in the range $0.2 \leqslant v \leqslant 0.5$. This criterion can be expressed as (see for example Fischer-Cripps, 2000)

$$Y = \sigma_{\mathrm{eq}} = \left\{\frac{1}{2}\left[(\sigma_1-\sigma_2)^2 + (\sigma_2-\sigma_3)^2 + (\sigma_1-\sigma_3)^2\right]\right\}^{1/2} \tag{6}$$

where σ_1, σ_2 and σ_3 are the principal stresses, σ_{eq} is the equivalent von Mises stress and Y is the yield strength of the sphere material. It can be easily seen that for the stress field given in Eq. (5), the coordinate axes are the principal directions. Hence, using Eq. (5), the equivalent von Mises stress at any location on the z axis can be expressed as follows:

$$\sigma_{\mathrm{eq}} = \sigma_{\mathrm{r}} - \sigma_z = p_{\mathrm{m}}\left\{\frac{3}{2}\left(1+\frac{z^2}{a^2}\right)^{-1} - (1+v)\left[\left(1-\frac{z}{a}\tan^{-1}(a/z)\right)\right]\right\} \tag{7}$$

Differentiating Eq. (7) with respect to the ratio z/a and equating to zero yields the dimensionless location, $\zeta_0 = z_0/a$, of the maximum equivalent stress in the form

$$(1+v)\left[\tan^{-1}(1/\zeta_0) - \frac{\zeta_0}{1+\zeta_0^2}\right] - \frac{3\zeta_0}{(1+\zeta_0^2)^2} = 0 \tag{8}$$

This location, in accordance with Eq. (6) marks the inception of yield. Eq. (8) can be rewritten as

$$v = \frac{3\zeta_0}{(1+\zeta_0^2)^2}\left[\tan^{-1}(1/\zeta_0) - \frac{\zeta_0}{1+\zeta_0^2}\right]^{-1} - 1 \tag{9}$$

Expanding the right-hand side of Eq. (9) to a Taylor series around the value $\zeta_0 = 0.5$, which corresponds to the dimensionless yielding inception depth for a typical ductile material with Poisson's ratio of about 0.3 (see Johnson, 1985), we obtain

$$v = 0.3576 + 3.000(\zeta_0 - 0.5) - 0.4448(\zeta_0 - 0.5)^2 + \cdots \tag{10}$$

From the first two terms in Eq. (10), an approximate linear relation between the dimensionless yielding inception depth and the Poisson's ratio is obtained in the form

$$\zeta_0 = 0.381 + v/3 \tag{11}$$

The error introduced by Eq. (11) was calculated from the remainder of the two first terms in the Taylor series of Eq. (10) and found to be less than 0.081%.

From Eq. (11) it can be seen that ζ_0 increases with v and hence, higher ductility results in yield inception on the axis of symmetry, deeper below the contact area.

Substituting ζ_0 for z/a in Eq. (7) and using Eqs. (1) and (4), we obtain the critical interference, ω_c, at yield inception in the form

$$\omega_c = \left[C_v \frac{\pi(1-v^2)}{2}\left(\frac{Y}{E}\right)\right]^2 R \tag{12}$$

where C_v is a function of the Poisson's ratio in the form

$$C_v = \left\{\frac{3}{2}(1+\zeta_0^2)^{-1} - (1+v)\left[1 - \zeta_0 \tan^{-1}\left(\frac{1}{\zeta_0}\right)\right]\right\}^{-1} \tag{13}$$

Using Eq. (11) for ζ_0 in Eq. (13) and expanding the right-hand side of Eq. (13) to a Taylor series around the value $v = 0.35$, which is the mean value of the Poisson's ratio in the range $0.2 \leqslant v \leqslant 0.5$, gives

$$C_v = 1.674 + 1.256(v - 0.35) + 0.611(v - 0.35)^2 + \cdots \tag{14}$$

Finally, the first two terms in Eq. (14) yield an approximate linear relation in the form

$$C_v = 1.234 + 1.256v \tag{15}$$

The error introduced by Eq. (15) was calculated from the remainder of the two first terms in the Taylor series of Eq. (14) and found to be less than 1.18%. Eq. (15) which was derived here analytically gives very close results to the analogous numerical approximations: $C_v = 1.297 + 1.17v$ that was obtained by Chang (1986) (see also K in Chang et al., 1988) for $H = Y/0.35$, and $C_v = 1.295\exp(0.736v)$ which is given by Jackson and Green (2005).

Using Eq. (12) for ω_c in Eq. (1), the critical load at yield inception is

$$P_c = \frac{\pi^3}{6} C_v^3 Y \left(R(1-v^2)\frac{Y}{E}\right)^2 \tag{16}$$

The maximum contact pressure at yielding inception, p_{mc}, can be found by substituting $\omega = \omega_c$ in Eqs. (1) and (2) and using them together with Eq. (12) in Eq. (4), hence

$$p_{mc} = C_v Y \tag{17}$$

Eq. (17) provides an interesting and useful physical meaning of the dimensionless parameter C_v. As can be seen this parameter is simply the ratio of the critical maximum contact pressure at yield inception (which is the maximum compressive stress occurring anywhere) over the yield strength of the sphere material.

3.2. Failure inception of brittle materials ($0 \leqslant v \leqslant 0.25$)

The failure inception of brittle materials occurs when the maximum tensile stress reaches the failure strength of the material (the maximum tensile stress criterion, see for example Johnson et al., 1973). In the case of perfect slip, all the stress components are compressive except the radial stress on the sphere surface which at the very edge and outside of the contact is tensile. The distribution of this radial stress on the sphere surface, inside and outside the contact area, has the form (see Johnson, 1985)

$$\sigma_r = p_m\left\{\frac{1-2v}{3}(a^2/r^2)[1-(1-r^2/a^2)^{3/2}]-(1-r^2/a^2)^{1/2}\right\}, \quad r \leqslant a$$
$$\sigma_r = p_m(1-2v)a^2/3r^2, \quad r > a \tag{18a}$$

with a maximum value at $r = a$ (which is the largest tensile stress anywhere)

$$\sigma^+_{max} = \sigma_r|_{r=a} = \frac{p_m(1-2v)}{3} \tag{18b}$$

This stress is responsible for the formation of ring cracks which are observed when brittle materials, like glass, are pressed into contact (see e.g., Johnson, 1985; Johnson et al., 1973).

Substituting the value of p_m from Eq. (4) into Eq. (18b) and using Eq. (1), we can express the critical interference ω_{cf} at brittle failure inception, in the case of perfect slip

$$\omega_{cf} = \left(\frac{F}{E}\right)^2\left[\frac{3\pi(1-v^2)}{2(1-2v)}\right]^2 R \tag{19}$$

where F is the failure tensile strength of the sphere material.

The critical load at the inception of brittle failure is obtained by using ω_{cf} in Eq. (1), thus

$$P_{cf} = \frac{9\pi^3 F}{2(1-2v)}\left[R\left(\frac{1-v^2}{1-2v}\right)\frac{F}{E}\right]^2 \tag{20}$$

4. The finite elements model for full stick condition

The available analytical solutions of the spherical contact problem under full stick condition are either approximate (see Goodman, 1962; Johnson et al., 1973; Hills and Sackfield, 1987), or cumbersome and incomplete (see Spence, 1968). To alleviate this drawback a finite element numerical solution, using a commercial package ANSYS 8.0, was employed.

The model is shown schematically in Fig. 2. For ductile materials the finite element mesh consisted of 9081 six-node triangular elements comprising a total of 29,277 nodes. The sphere was divided into three different mesh density zones (see Fig. 2(a)), where zones III and II were within $0.015R$ and $0.1R$, respectively, from the sphere summit, and zone I outside the $0.1R$ distance. Zone III had the finest mesh and

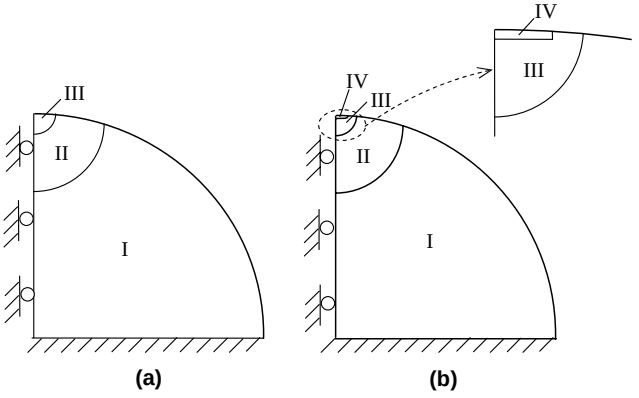

Fig. 2. The finite elements model: (a) for a ductile material and (b) for a brittle material.

it covered the whole contact area as well as the location of the first yield for all the solved cases. The other zones had gradual coarser mesh at increasing distance from the sphere summit.

Ductile materials with different mechanical properties were analyzed to study their effect on the yield inception. The ratio E/Y covered a wide range from 200 to 1000, typical for metals. The Poisson's ratio v varied in the range from 0.2 to 0.5, typical for ductile materials. The von Mises yielding criterion was used to detect the onset of plastic deformation. The interference δ was gradually increased and the equivalent von Mises stress σ_{eq} at each node was checked against the material yield strength Y. The interference $\delta = \delta_c$ is the smallest one at which $\sigma_{eq} = Y$ at least in one node and this case corresponds to the yield inception in stick. It provides all the critical values like the critical interference, δ_c, critical load, L_c, the radius of the contact area a_c, and the location of the yield inception.

For brittle materials zone III was subdivided so that a very thin layer (see zone IV in Fig. 2) was added at a very close proximity to the contact area. This zone had the finest mesh, its thickness was $7.5 \cdot 10^{-4}R$ and it had a width of $0.01R$ so that it contained the location of the first failure inception on the contact area. The whole mesh for brittle materials consisted of 10,412 six-node triangular elements comprising 31,322 nodes.

The Poisson's ratio, v, for brittle materials varied in the range from 0 to 0.25 and the ratio E/F covered the range from 4000 to 16,000. The maximum tensile stress criterion was used to detect the onset of brittle failure. This was done with an identical procedure as for ductile materials and provided the critical values for brittle failure inception i.e., δ_{cf}, L_{cf}, a_{cf}, and the location of the brittle failure inception.

5. Results and discussion

Firstly, it was found that for both ductile and brittle materials the contact conditions have a very small effect on the radius of the contact area, a, i.e., its value in full stick can be fairly evaluated by Eq. (2), with δ instead of ω.

5.1. Ductile materials ($0.2 \leqslant v \leqslant 0.5$)

As will be shown later (see discussion of Fig. 8) the critical interference in stick can be related to that in slip by $\delta_c \leqslant \omega_c$. Hence, for the interference $\omega = \delta_c$, Eqs. (1)–(4) are valid under slip condition. This allows comparing behavior at yield inception in stick with that at identical interference in slip. The distribution over the contact area of the dimensionless pressure, p/Y, and tangential stress τ_{rz}/Y at the inception of yield in stick, δ_c, are shown in Figs. 3 and 4, respectively for ductile materials for $v = 0.2, 0.3, 0.4$. The solid and dashed lines in Fig. 3 correspond to the cases of full stick and perfect slip, respectively. The results for the full stick were obtained by the numerical method described above while the pressure distribution for the perfect slip was obtained analytically from Eqs. (1) to (4) with $\omega = \delta_c$. As shown in Fig. 3 the pressure level, and hence the critical load L_c, decreases with decreasing v. Also at a small value of the Poisson's ratio ($v = 0.2$) the pressure distribution in stick is appreciably different than in slip for the same interference $\omega = \delta_c$. This is because of high tangential stresses in the contact surface under the stick condition (see Fig. 4 at $v = 0.2$). At higher values of the Poisson's ratio the tangential stresses in the contact interface in stick are much lower than the corresponding pressure (see Figs. 3 and 4 at $v = 0.4$) and therefore the pressure distributions in stick and in slip are similar (see Fig. 3 at $v = 0.4$).

Fig. 5 presents the distribution over the contact area of the dimensionless equivalent von Mises stress σ_{eq}/Y at yield inception in stick. As can be seen the equivalent stress has two maxima, the lower one close to the edge of the contact area at $r/a \approx 0.9$ results from the high tangential stresses there (see Fig. 4) while the absolute maximum occurs at $r/a = 0$ for the full range of the Poisson's ratio. From the location of the absolute maximum of σ_{eq} it is clear that the yield inception of ductile materials in either full stick or perfect slip contact always occurs on the axis of symmetry.

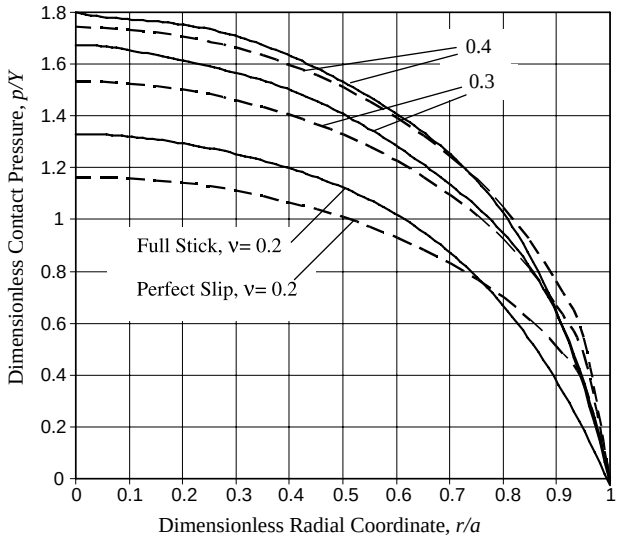

Fig. 3. The dimensionless pressure, p/Y, over the contact area at yield inception in stick.

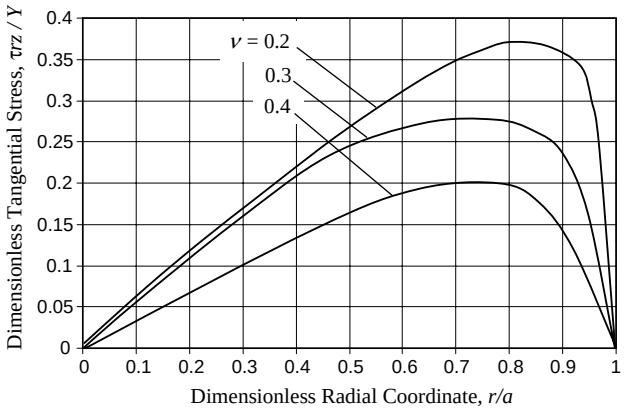

Fig. 4. The dimensionless tangential stress, τ_{rz}/Y, over the contact area at yield inception in stick.

Fig. 6 presents the distribution along the axis of symmetry of the dimensionless equivalent von Mises stress σ_{eq}/Y at yield inception in stick. As can be seen from the figure the maximum value, $\sigma_{eq}/Y = 1$ and hence, the location of yield inception, occurs closer to the contact with decreasing values of the Poisson's ratio. For $v = 0.4$ and 0.3 the location of this maximum beneath the contact is at $z/a = 0.45$ and $z/a = 0.3$, respectively while for $v = 0.2$ the yield inception in stick is at the contact area ($z/a = 0$).

A comparison between the dimensionless locations of yielding inception, ζ_0, as a function of the Poisson's ratio in stick ($\delta = \delta_c$) and in slip ($\omega = \omega_c$) is presented in Fig. 7. The linear behavior in slip is according with Eq. (11) and the results in stick are those obtained from the numerical solution where the yield inception location is identified as was shown in Fig. 6. From Fig. 7 it can be seen that for $v \leqslant 0.26$ the yield inception in stick occurs at the contact surface, while in slip it always occurs beneath the contact surface. As v increases the yielding inception depth ζ_0 in stick grows faster than that in slip,

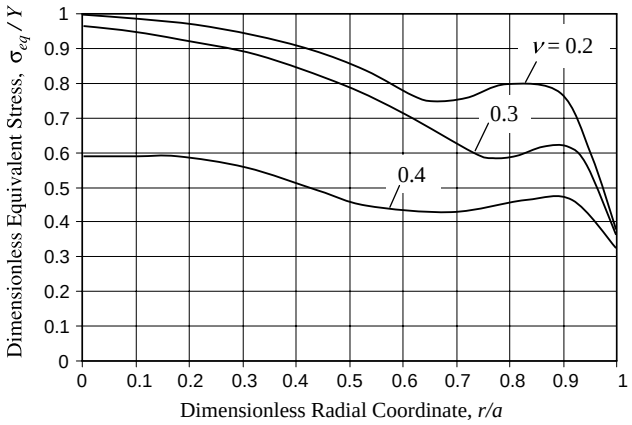

Fig. 5. The dimensionless equivalent stress, σ_{eq}/Y, over the contact area at yield inception in stick.

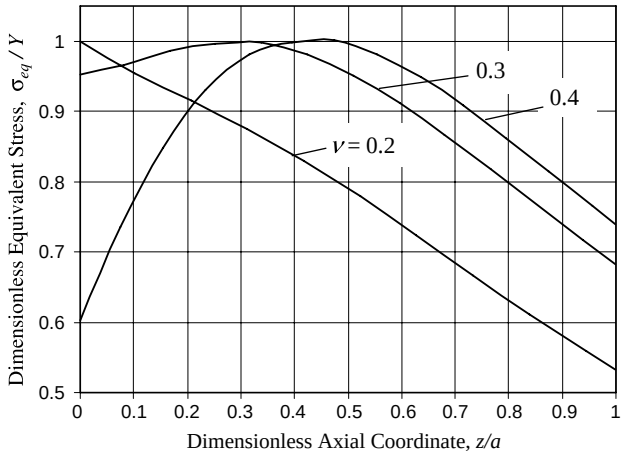

Fig. 6. The dimensionless equivalent stress, σ_{eq}/Y, along the axis of symmetry in stick.

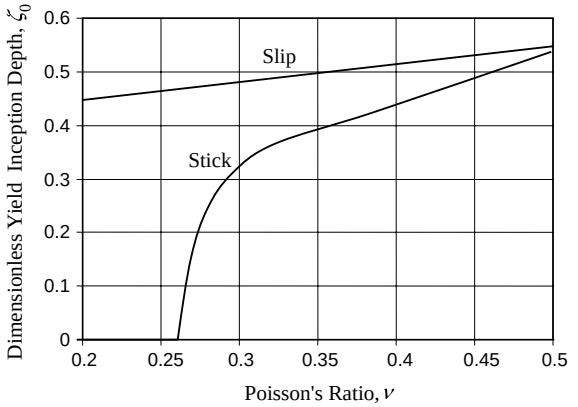

Fig. 7. The dimensionless yield inception depth, ζ_0, vs. Poisson's ratio—in stick and in slip.

approaching the later and finally for $v = 0.5$ becoming identical to it. The ratio, ζ_0^*, of yielding inception depth in stick over that in slip is well approximated by the following function of the Poisson's ratio:

$$\begin{aligned} &\zeta_0^* = 0, \quad v \leqslant 0.26 \\ &\zeta_0^* = 1.54(v - 0.26)^{0.294}, \quad 0.26 < v \leqslant 0.5 \end{aligned} \tag{21}$$

Fig. 8 presents the ratios of the critical interference (δ_c/ω_c) and critical load (L_c/P_c) for yielding inception in full stick over that in perfect slip. These ratios were calculated for the wide range of E/Y values from 200 to 1000 and found to be independent of the material properties except for the Poisson's ratio. For small values of v, the critical interference and the critical load in stick are considerably less than the same parameters in slip. This is because of high tangential stresses in the contact interface under stick that are non existent under slip condition. For high values of the Poisson's ratio the tangential stresses under stick condition are low enough to make the critical interference and critical load in stick and in slip similar. The ratios of the critical interference and critical load are well approximated by the following functions of v in the range $0.2 \leqslant v \leqslant 0.5$:

$$\delta_c/\omega_c = 6.82v - 7.83(v^2 + 0.0586) \tag{22}$$

$$L_c/P_c = 8.88v - 10.13(v^2 + 0.089) \tag{23}$$

5.2. Brittle materials ($0.1 \leqslant v \leqslant 0.25$)

In analyzing the failure inception for brittle materials it was found that $\delta_{cf} \gg \omega_{cf}$ namely, the failure inception in stick occurs at a much higher interference than in slip. This finding is in agreement with the results reported by Johnson et al. (1973) for a sphere contacting a rigid flat, and it shows a behavior that is completely different from that in the previous ductile material case where $\delta_c \leqslant \omega_c$. To demonstrate this behavior we show in Fig. 9 the distributions over the sphere surface (both inside and outside the contact area) of the dimensionless radial stress, σ_r/F, in both stick and slip. The results are shown for $v = 0.1$ and for the same interference $\delta = \omega_{cf}$. The critical interference in slip, ω_{cf}, and the corresponding distribution, σ_r/F, were obtained from Eqs. (19) and (18a), respectively. As can be seen from Fig. 9 the dangerous tensile portion of σ_r/F is much higher in slip than in stick. Another important observation is that the maximum value of σ_r/F, and hence the failure inception in stick occurs outside the contact area while that in slip

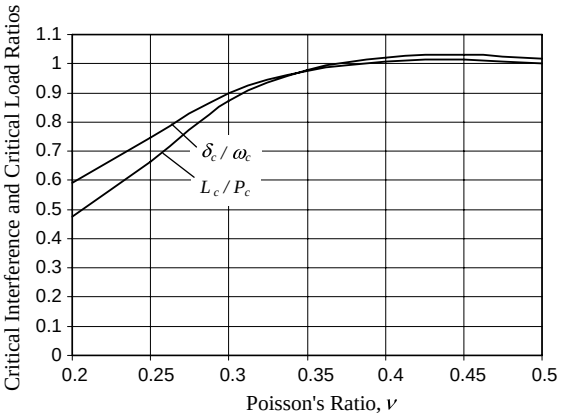

Fig. 8. The ratios of the critical interference, δ_c/ω_c, and critical load, L_c/P_c, for yielding inception of ductile materials in full stick over perfect slip.

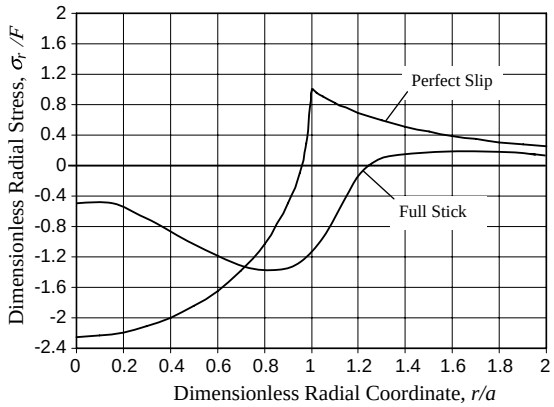

Fig. 9. Distribution of the dimensionless radial stress, δ_r/F, on the sphere surface, in stick and slip for $v = 0.1$, $\delta = \omega_{cf}$.

always occurs at the edge of the contact area $r/a = 1$. Similar results were obtained for other v values showing that in stick the failure inception slightly moves from $r/a = 1.49$ to $r/a = 1.56$ as v increases from 0.1 to 0.25. The failure inception in slip always occurs at the edge of the contact area $r/a = 1$, see Eq. (18b). The lower level of σ_r/F in stick compared to that in slip outside the contact area, as shown in Fig. 9 for $r/a > 1$, is probably due to the constraint imposed on the radial displacement of points on the sphere surface as they engage the rigid flat. This result is in agreement with the approximate solution and explanation provided by Johnson et al. (1973).

The critical interference for brittle failure inception in stick, δ_{cf}, and the critical load L_{cf} were obtained for a wide range of material properties in terms of the ratio E/F as described in Section 4 above. It was

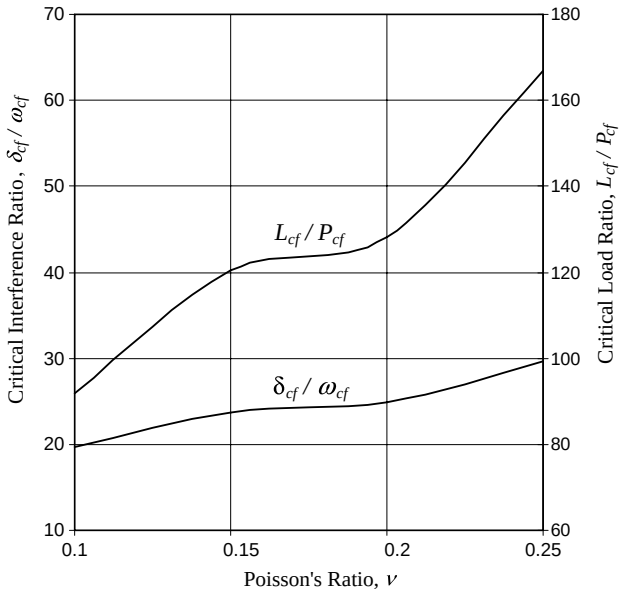

Fig. 10. The ratios of the critical interference, δ_{cf}/ω_{cf}, and critical load, L_{cf}/P_{cf}, for failure inception of brittle materials in full stick over perfect slip.

found that, like the ratios of the critical interference, δ_c/ω_c, and critical load, L_cP_c, for yielding inception (see Fig. 8), the analogous ratios for brittle failure inception in stick over that in slip, δ_{cf}/ω_{cf} and L_{cf}/P_{cf} are also independent of the material properties except for the Poisson's ratio. Fig. 10 presents the ratios of the critical interference δ_{cf}/ω_{cf} and critical load L_{cf}/P_{cf} as functions of v. It can be seen that for brittle materials the critical interference and load in stick are much larger than in slip. In the range $v = 0.1$–0.25 the ratio δ_{cf}/ω_{cf} varies from 20 to 30 while the ratio L_{cf}/P_{cf} varies from 90 to 165.

Finally an interesting observation for both ductile and brittle materials is that the ratio L/P is very well related to δ/ω by $L/P = (\delta/\omega)^{3/2}$ throughout the elastic contact regime. Hence, the load–interference behavior in stick is similar to that in slip (see Eq. (1)).

6. Conclusion

We studied the effect of contact condition and material properties on the termination of elasticity in spherical contact by comparing plastic yield and brittle failure inceptions in stick and slip.

With ductile materials the yield inception always occurs at a single point on the axis of symmetry. At smaller values of the Poisson's ratio the behavior in stick is much different than in slip because of high tangential stresses in the contact interface under the stick condition. As a result the values of critical interference, critical load, and yielding inception depth in stick are lower than their corresponding values in slip. At higher values of the Poisson's ratio the tangential stresses under stick condition are low and the yield inceptions in stick and slip are similar.

With brittle materials the failure inception always occurs on the circumference of a circle on the sphere surface. The values of critical interference, critical load, and radial location of failure inception in stick are larger than their corresponding values in slip, contrary to the behavior of ductile materials. In slip the failure incepts at the edge of the contact area while in stick this happens outside the contact area. For both ductile and brittle materials the ratios of critical interference and critical load in full stick over that in perfect slip depend solely on the Poisson's ratio and can be presented as simple expressions of this parameter. Also, the load–interference behavior in stick is similar to that in slip in that the load is proportional to a 3/2 power of the interference.

Acknowledgement

This research was partially supported by The Israel Science Foundation.

References

Adams, G.G., Nosonovsky, M., 2000. Contact modeling—forces. Trib. Int. 33, 431–442.

Bryant, M.D., Keer, L.M., 1982. Rough contact between elastically and geometrically identical curved bodies. J. Appl. Mech. ASME 49, 345–352.

Chang, W.R., 1986. Contact, adhesion and static friction of metallic rough surfaces. Ph.D. thesis, University of California, Berkeley.

Chang, W.R., Etsion, I., Bogy, D.B., 1988. Static friction coefficient model for metallic rough surfaces. J. Tribol. ASME 110, 57–63.

Etsion, I., Kligerman, Y., Kadin, Y., 2005. Unloading of an elastic–plastic loaded spherical contact. Int. J. Solids Struct. 42 (13), 3716–3729.

Fischer-Cripps, A.C., 1997. Predicting Hertzian fracture. J. Mater. Sci. 32, 1277–1285.

Fischer-Cripps, A.C., 2000. Introduction to Contact Mechanics. Springer, New York.

Goodman, L.E., 1962. Contact stress analysis of normally loaded rough spheres. ASME J. Appl. Mech. 29, 515–522.

Hamilton, G.M., 1983. Explicit equations for the stresses beneath a sliding spherical contact. Proc. Inst. Mech. Eng. 197C, 53–59.

Hills, D.A., Sackfield, A., 1987. The stress field induced by normal contact between dissimilar spheres. J. Appl. Mech. ASME 54, 8–14.

Jackson, R.L., Green, I., 2005. A finite element study of elasto-plastic hemispherical contact against a rigid flat. J. Tribol. ASME 127, 343–354.

Johnson, K.L., 1985. Contact Mechanics. Cambridge University Press, Cambridge, MA.

Johnson, K.L., O'Connor, J.J., Woodward, A.C., 1973. The effect of the indenter elasticity on the Hertzian fracture of brittle materials. Proc. Roy. Soc. Lond. A334, 95–117.

Kogut, L., Etsion, I., 2002. Elastic–plastic contact analysis of a sphere and a rigid flat. J. Appl. Mech. ASME 69, 657–662.

Kogut, L., Etsion, I., 2003. A semi-analytical solution for the sliding inception of a spherical contact. J. Trib. ASME 125, 499–506.

Kosior, F., Guyot, N., Maurice, G., 1999. Analysis of frictional contact problem using boundary element method and domain decomposition method. Int. J. Numer. Methods Eng. 46, 65–82.

Mindlin, R.D., 1949. Compliance of elastic bodies in contact. J. Appl. Mech. ASME 16, 259–268.

Spence, D.A., 1968. Self-similar solutions to adhesive contact problems with incremental loading. Proc. Roy. Soc. Lond. A305, 55–80.

Spence, D.A., 1975. The Hertz contact problem with finite friction. J. Elasticity 5, 297–319.

Zhang, H., Chang, L., Webster, M.N., Jackson, A., 2003. Effects of friction on the contact and deformation behavior in sliding asperity contacts. Tribol. Trans. 46, 514–521.

Zhupanska, O.I., Ulitko, A.F., 2005. Contact with friction of a rigid cylinder with an elastic half-space. J. Mech. Phys. Solids 53 (5), 975–999.